Moisture and Salinity Distribution under Artificial Intelligence-Based Systems and Traditional Farming Practices, and Their Influence on Yellow Corn Yield

Mustafa Hussein Salih[1], Mohammed Ali Abood[2], Ahmad S. Abdullah[3]

[1,2,3] Department of Soil Science and Water Resources, College of Agriculture, University of Diyala, Iraq
Emails: mustafahusen1989@gmail.com[1], Mohammed.Ali.Abood@uodiyala.edu.iq[2], ahmed.alogaidi28@gmail.com[3]

Abstract

This study was conducted at the research station of, College of Agriculture, University of Diyala, during the summer growing season of 2025. It aimed to optimize water consumption for maize by comparing a traditional irrigation system with a smart irrigation system supported by artificial intelligence technologies. It also evaluated the impact of two soil moisture levels (50% and 75% of field capacity) on water consumption, water use efficiency, crop yield. The smart irrigation system relied on soil moisture sensors (TDT) for automated irrigation control, while the traditional irrigation system was operated manually. The entire irrigation system was powered by solar energy. The moisture distribution analysis outcomes under the drip irrigation system showed a clear spatial gradient in soil moisture content. The highest moisture ratios were concentrated near by the emitters and within the surface layers, then gradually decreased with horizontal distance from the water source and with increasing depth. By optimizing irrigation timing and volume based on sensor-driven data, the smart irrigation system ensured more consistent moisture distribution across the root zone compared to traditional practices. Regarding salinity distribution. The lowest salinity levels were recorded near the drip emitters, attributed to the continuous leaching of salts by irrigation water. Conversely, salt concentrations gradually increased toward the periphery of the wetting front and in areas distant from the water source, driven by water-driven salt transport and subsequent accumulation at the wetting front boundaries. Furthermore, precise irrigation management through use the smart system helped reduce salt accumulation within the root zone compared to the traditional system.

Keywords: *Zea mays* L. Artificial Intelligence, Soil Moisture Distribution, Soil Salinity Distribution, Soil Moisture Sensor.

Introduction

In light of the growing challenges that facing the agricultural sector, particularly in areas suffering from water scarcity and shrinking arable land (Sharma *et al.,* 2020). the need to adopt smart solutions that ensure optimal water use and sustainable agricultural production has become urgent (Gaitan *at el.*,2025). Artificial intelligence (AI) is one of the most prominent solutions in this regard, providing advanced analytical tools and decision support systems that help improve resource management efficiency (Montzka،2026) . AI has also aided in water planning and management through the use of smart irrigation systems to optimize water use in agriculture, which is one of the largest users of this resource (Ghazi *et al.,* 2025). The system analyzes data on soil moisture, surrounding weather conditions, and other variables. As is known, water consumption varies from one soil type to another, as does the soil's water retention rate, depending on its texture and structure (Faleh et al., 2023). AI can provide more accurate data for decision-making, thereby reducing water waste. Examples include real-time monitoring and control of water management, response to changes in water levels, and mobile applications that use AI to provide accurate, real-time data on soil water levels (Salam, 2023).

Soil salinity and moisture distribution in the root zone are among the most critical factors in determining crop yield and production when discussing drip irrigation (Nurmalitasari *et al.,* 2025). Soil salinity increases with horizontal and vertical distance from the emitter center, with the highest salt accumulation occurring at the horizontal and vertical wett zones. This accumulation increases with shorter irrigation intervals and higher irrigation volumes. High-flow emitters are more effective at removing salts from the root zone compared to low-flow emitters (Al-Saadoun, 2006).

The basis behind this study

This study was conducted to develop a smart, solar-powered irrigation system that utilizes intelligent sensing and control technologies to manage irrigation water within the field. The notion of this study is grounded in the utilization of soil moisture sensors to obtain real-time data regarding the water status within the root zone, thereby allowing accurate irrigation management and effective salt leaching control. This data is then transmitted to an electronic control unit that automatically makes irrigation decisions

according to predetermined moisture limits for each treatment, instead of relying on traditional irrigation based on fixed schedules**.**

Methodology

Installing soil sensors

In this study, soil moisture sensors that operate on the principle of time frequency were used. They are characterized by their resistance to rust and corrosion, as well as their ability to display readings continuously through an integrated digital screen, as shown in (Figure 1). These sensors measure soil moisture periodically every ten minutes, and also allow reading soil temperature and electrical conductivity, in addition to the possibility of giving a manual start command when needed and displaying it on a digital

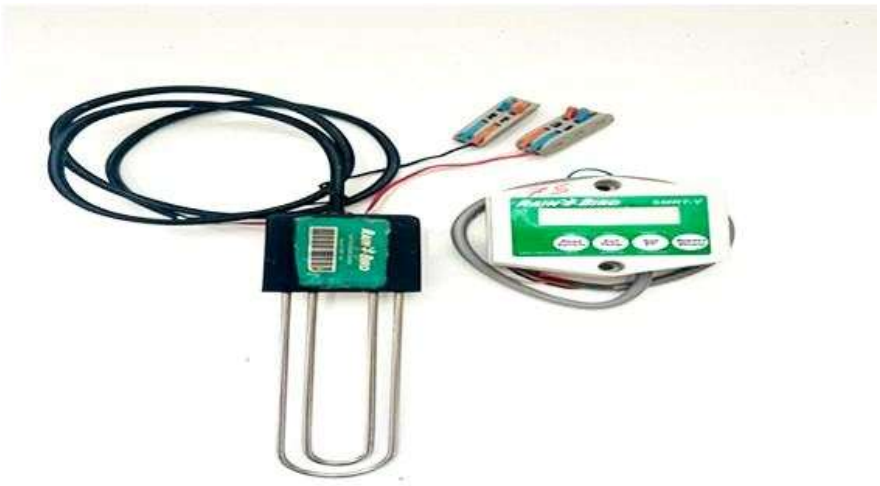

Figure 1. Moisture sensors.

screen containing four buttons. The system comprises four functional control buttons: the first triggers an immediate measurement of soil moisture, overriding the standard ten-minute polling interval. The second and third buttons initiate readings for soil temperature and electrical conductivity, respectively. The fourth one works as a manual override, activating the irrigation valve and pump to bypass the sensor-defined thresholds. Operating limits had set based on field capacity and in accordance with soil texture, according to the sensor manual and as shown in Table (1). Before installation in the field, the sensors were tested for two days to verify their efficiency and reading accuracy. The sensor-derived moisture readings had authenticated against the standard gravimetric method. The outcomes revealed minimal deviations, with differences in some instances not exceeding 1%, thereby confirming the accuracy and suitability of the sensors for field applications."

Table 1. Field capacity of different soil textures

Soil Type	(Typical Field Capacity)	(Suggested Moisture Threshold)
(Sand)	15%	12%
Loamy Sand	18%	14%
Sandy Loam	21%	17%
Sandy Clay Loam	29%	23%
Loam	31%	25%
Sandy Clay	33%	26%
Silt Loam	35%	28%
Clay Loam	36%	29%
Silt	38%	30%
Silty Clay	40%	32%
Silty Clay Loam	40%	32%
Clay	44%	35%

Moisture distribution

The moisture content was estimated by the gravimetric method during the flowering stage. Soil samples were taken during the growth stages mentioned above using a special moisture sampling ochre with a diameter of 1.25 cm. After 48 hours of irrigation, at depths of 0-10, 10-20, and 20-30 cm horizontally and vertically from the dripper, the samples were dried in the oven at 105 degrees Celsius for 24 hours. The percentage of moisture was calculated based on dry weight according to the method mentioned by Richards (1954). Surfer software version 2025 was used to draw the contour lines of the moisture distribution.

Salt distribution

The salinity distribution of the different experimental treatments was measured during the flowering stage or Blooming Stage and at the same depths as before using a special moisture sampling chuck with a diameter of 1.25 cm. These samples were then dried in an oven at 105°C. The entire soil samples were ground and passed through a sieve with a diameter of 2 mm. A 1:1 soil extract was prepared, and the electrical conductivity was measured using an EC-meter. Surfer software version 2025 was used to draw the contour lines of the salinity distribution.

Results and discussion

Moisturizing distribution

The results shown in Figure 2 illustrate the moisture distribution for the conventional irrigation treatment of 50% (CM1) of the field capacity in the first replicate. The highest gravimetric water content was recorded below the center of the dripper, reaching 30.7%. This percentage decreased to 30% at a depth of 15 cm and remained the same at a depth of 30 cm below the dripper, which supports the saturation of the area below the dripper with water. When moving horizontally at a distance of 15 cm, the gravimetric water content in the surface layer decreased to 27.6%, and the decrease for this distance gradually increased with depth until it recorded 27.6% and 25.4% at depths of 15 cm and 30 cm, respectively. While moving horizontally at a distance of 30 cm from the center of the dripper, the gravimetric water content was recorded at 24.3% and decreased gradually with depth, reaching 23.3% and 21.4% at depths of 15 cm and 30 cm, respectively. In the Second replicate, the highest gravimetric water content was recorded below the center of the dripper, reaching 28.4%. This ratio declined to 27.7% at a depth of 15 cm and recorded a slight decrease at a depth of 30 cm, where it reached 27.6%. When moving horizontally at a distance of 15 cm, the gravimetric water content in the surface layer decreased to 27.3% and remained the same at a depth of 15 cm. The decrease for this distance gradually increased with depth until it was recorded at a depth of 30 cm at 27%. But when moving horizontally at a distance of 30 cm from the center of the dripper. The gravimetric water content was recorded at 26.2 cm and decreased gradually with depth, reaching 25.9% and 25% for the depths of 15 cm and 30 cm. In the third replicate, the highest T gravimetric water content was recorded below the center of the emitter, reaching 26.4%. This ratio declined to 24.9% at a depth of 15 cm and showed a slight decrease at a depth of 30 cm, reaching 24.7%. By moving horizontally 15 cm away, the The gravimetric water content in the surface layer decreased to 24.3% and continued to decrease, recording 23.8% at a depth of 15 cm. The decrease gradually increased with depth, reaching 23.7% at a depth of 30 cm. When moving horizontally 30 cm away from the center of the emitter, the gravimetric water content was recorded at 22.5% and increased slightly at a depth of 15 cm to 22.6%,This was also indicated by (Zhang et el,2022). This increase is attributed to the accumulation of organic matter at this depth when it was mixed into the soil at the beginning of the season.

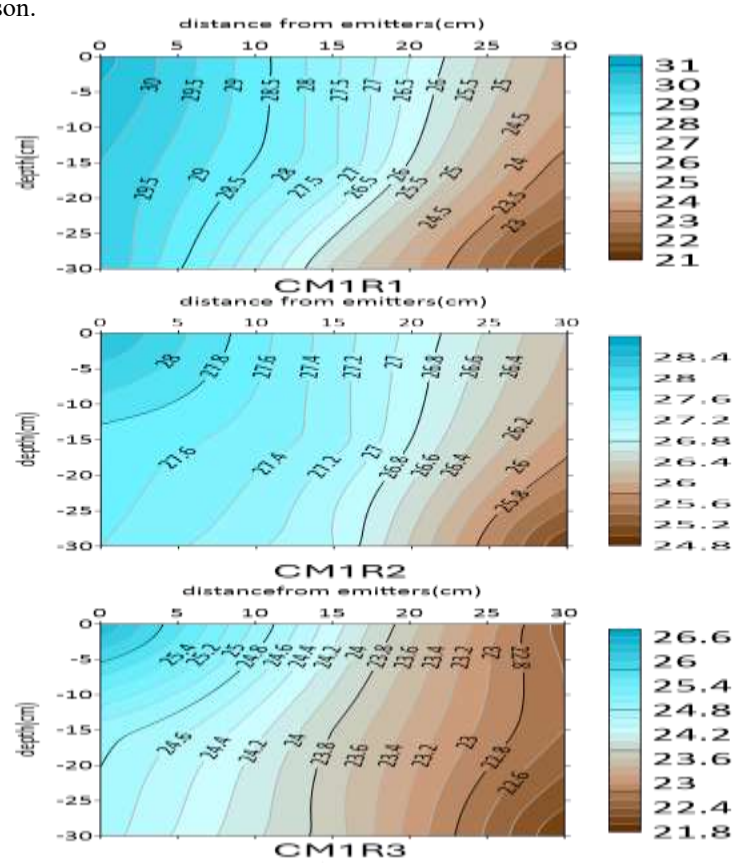

The gravimetric water content gradually declined, reaching 22% at a depth of 30 cm. "The figure illustrates that conventional irrigation at 50% field capacity results in a clear wetting front. Moisture distribution is non-uniform, being highest near the emitter and decreasing with increasing horizontal distance. Furthermore, the horizontal variation in moisture was more pronounced than the vertical variation. This indicates that distance from the emitter was the most influential factor in water distribution within the studied area. This suggests that traditional irrigation at this ratio may not guarantee a balanced distribution of moisture across the entire root zone, particularly at the furthest points from the emitters. The results confirm that relying on traditional irrigation at 50% of field capacity can lead to areas of suitable moisture near the water source, compared to areas of lower moisture at the edges. This can cause uneven water absorption and plant growth. Therefore, improving the uniformity of distribution requires adjusting the spacing between emitters, the drainage rate, and the irrigation time. It may also necessitate adopting smart irrigation systems or precise scheduling based on actual soil moisture rather than relying solely on a fixed percentage of field capacity.

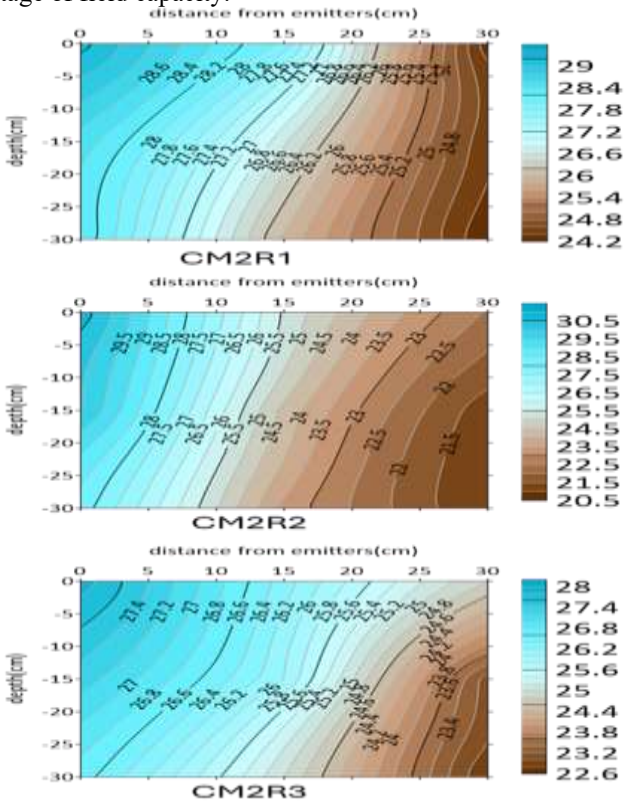

Figure 2. Moisture distribution under conventional irrigation at 50% of field capacity.

The results shown in Figure 3 illustrate the moisture distribution for the conventional irrigation treatment at 75% (cm²) of field capacity. In the first replicate, the highest gravimetric water content was recorded below the center of the emitter, reaching 29.7%. This ratio decline to 28.51% at a depth of 15 cm and showed a slight decrease at a depth of 30 cm, reaching 28.37% below the emitter. At a horizontal distance of 15 cm, the gravimetric water content in the surface layer decline to 27.94%, and this decrease gradually increased with depth, reaching 26.64% and 25.95% at depths of 15 cm and 30 cm, respectively "At a horizontal distance of 30 cm from the emitter, the gravimetric water content was recorded at 24.27%. This value increased slightly to 24.45% at a depth of 15 cm, a trend potentially attributed to the accumulation of organic matter at this depth." At a depth of 30 cm, the lowest gravimetric water content was recorded at 24.22%. In the second replicate the highest the gravimetric water content was recorded below the center of the dripper, reaching 30.78%. This percentage ratio decline to 30.06% at a depth of 15 cm and recorded a further decrease at a depth of 30 cm, reaching 28.27% below the dripper. When moving horizontally at a distance of 15 cm, the gravimetric water content in the surface layer decreased to 25.42%, and the decrease for this distance gradually increased with depth until it recorded 24.33% and 23.34% for depths of 15 and 30 cm respectively. When moving horizontally at a distance of 30 cm from the center of the dripper, the weighted moisture content was recorded at 22.44% and decreased to a depth of 15 cm, reaching 21.2%, and at a depth of 30 cm.

In the third replicate, the highest Gravimetric water content was recorded below the center of the dripper, reaching 27.9%. This percentage decline to 26.3% at a depth of 15 cm and decreased further at a depth of 30 cm, reaching 24.8% below the dripper. By moving horizontally 15 cm away, the Gravimetric water content in the surface layer reached to 27.3%, and the decrease gradually increased with depth, reaching 26% and 23.1% at depths of 15 cm and 30 cm, respectively. At a horizontal distance of 30 cm from the emitter, the gravimetric water content was 26.7%. As depth increased, moisture levels decreased to

25.0% at 15 cm and reached a minimum of 22.8% at a depth of 30 cm. This can be explained by the fact that contour maps show a clear spatial gradient in the studied characteristic, with high values concentrated on the left side and gradually decreasing towards the right side. The intensity of this gradient varies between treatments, reflecting the influence of regulating physical factors. As well as this behavior reveals the impact of the physical properties governing the movement of water, heat, or matter within the soil medium, such as porosity, texture, bulk density, and hydraulic conductivity, as well as the location of the source. Furthermore, the conjunction of contour lines in definite areas indicates a high ratio of spatial change, whereas their divergence reflects a more stable and homogeneous state.

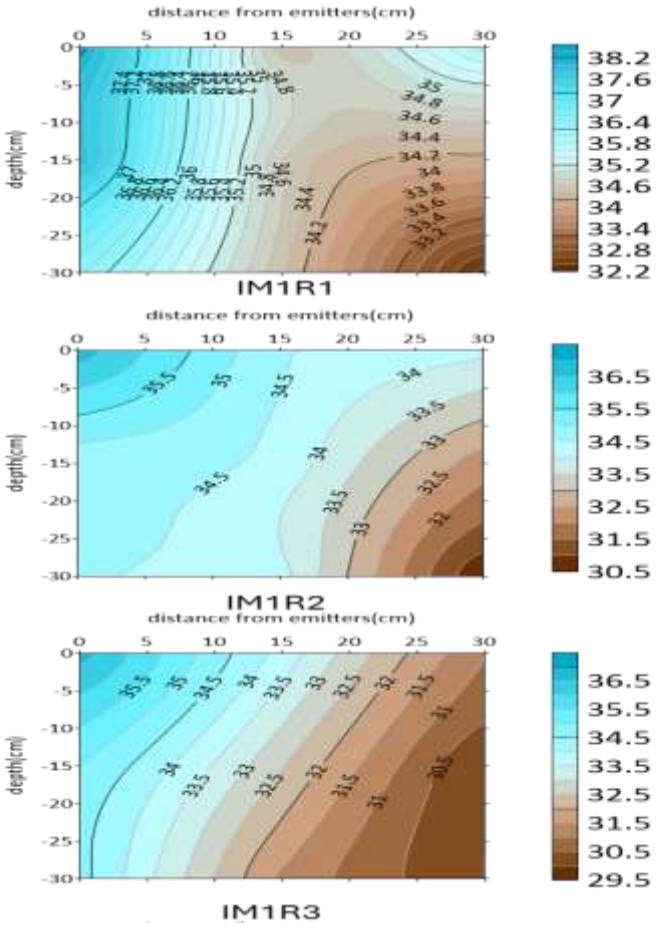

Figure 3. Moisture distribution under conventional irrigation at 75% of field capacity

The outcomes shown in Figure 4 illustrate the moisture distribution of the smart irrigation treatment at 50% of the field capacity in the first replicate. The highest Gravimetric water content was documented below the center of the dripper, reaching 38.3%. This percentage ratio decline with depth to 34.46% at a depth of 15 cm and increased to 35.9% at a depth of 30 cm below the dripper, which supports the accumulation of organic matter in this layer. When moving horizontally at a distance of 15 cm, the Gravimetric water content in the surface layer was recorded at 37.94%, and the decrease gradually with depth until it was recorded at 34.58% and 34.13% for the depths of 15 cm and 30 cm respectively. When moving horizontally at a distance of 30 cm from the center of the dripper, the Gravimetric water content was recorded at 36.44% and decreased gradually with depth to 34.44% and 32.3% for the depths of 15 cm and 30 cm respectively. In the second replicate, the highest the Gravimetric water content was documented below the center of the dripper, reaching 36.76%. This percentage ratio declined with depth to 34.55% at a depth of 15 cm and recorded a slight decrease at a depth of 30 cm, where it reached 34.12%. When moving horizontally at a distance of 15 cm, the Gravimetric water content in the surface layer decreased to 34.64%, and the decrease for this distance gradually increased with depth until it recorded 34.34% and 32.22% for the depths of 15 cm and 30 cm respectively. "At a horizontal distance of 30 cm from the emitter, the gravimetric moisture content was 34.59% at the surface, slightly decreasing to 34.17% at a 15 cm depth. The lowest moisture content, 30.52%, was recorded at a depth of 30 cm."As for the third replicate, the highest the Gravimetric water content was recorded below the

center of the dripper, reaching 36.71%. This ratio shrunk with depth to 33.82% at a depth of 15 cm and continued to decrease to 31.04% at a depth of 30 cm. When moving horizontally at a distance of 15 cm, the weighted moisture in the surface layer decreased to 34.99%. This decrease gradually increased with depth until it recorded 32.53% and 30% for depths of 15 cm and 30 cm respectively. When moving horizontally at a distance of 30 cm from the center of the dripper, the highest the Gravimetric water content was recorded at 34.64% and decreased gradually with depth to 31.37% and 30% for depths of 15 cm and 30 cm respectively. The witnessed spatial and temporal differences are governed by the Richards Equation, which characterizes water flux within unsaturated soil media. Water movement is driven by the total potential gradient; this gradient is primarily substantial, promoting quick infiltration, before it gradually attenuates as the system approaches equilibrium or is influenced by evapotranspiration. These outcomes stress that depending on generalized averages can lead to important errors in irrigation scheduling, highlighting the necessity of accounting for soil spatial heterogeneity. Furthermore, this study demonstrates how artificial intelligence can leverage moisture distribution mapping to facilitate site-specific irrigation, a practice supported by the findings of Jones (2004) and (Ma *et al.,* 2022) regarding the integration of spatial modeling and smart irrigation for water sustainability."

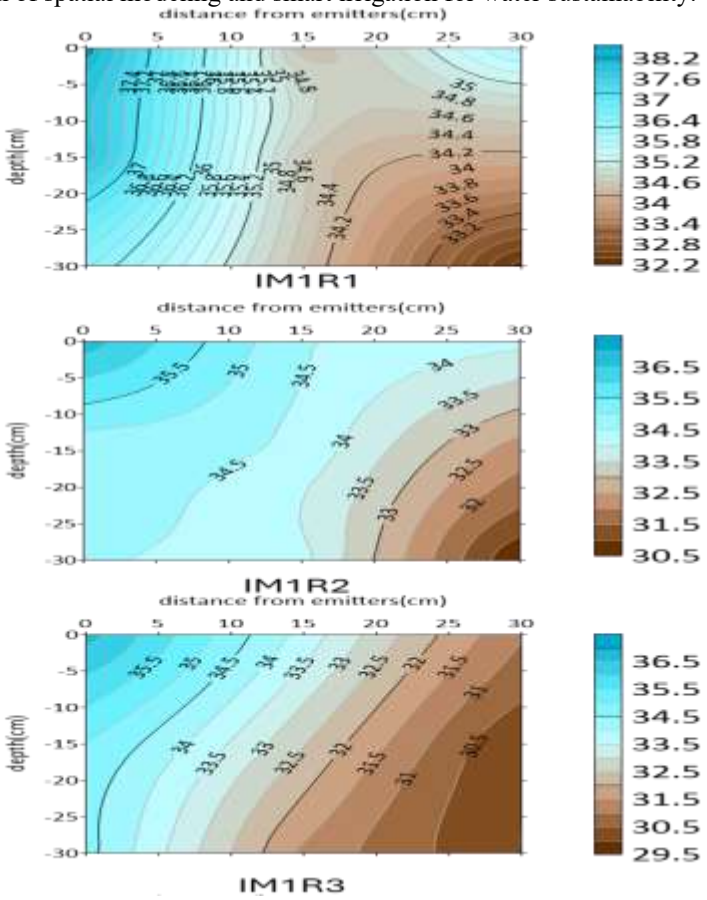

Figure 4. Displays the moisture distribution for the smart irrigation treatment at 50% of field capacity.

The results shown in Figure 5 illustrate the moisture distribution for the smart irrigation treatment (IM2). 75% of the field capacity in the first replicate recorded the highest weighted moisture below the center of the dripper, reaching 29.69%. This ratio decreased with depth to 28.95% and 27.72% at depths of 15 cm and 30 cm, respectively. When moving horizontally at a distance of 15 cm, the Gravimetric water content in the surface layer was recorded at 27.72%, and the decrease gradually increased with depth until it reached 27.48% and 27.42% for depths of 15 cm and 30 cm, respectively. When moving horizontally at a distance of 30 cm from the center of the dripper, the Gravimetric water content was recorded at 26.04%, and it gradually decreased with depth to 25.97% and 25.56% for depths of 15 cm and 30 cm, respectively. "In the second replication, the gravimetric moisture content directly beneath the emitter was 27.33% in the surface layer, followed by 27.36% and 27.19% at depths of 15 cm and 30 cm, respectively. At a horizontal distance of 15 cm from the emitter, the surface moisture content declined to 27.07%, with a gradual decline observed through the soil profile, reaching 26.70% and 26.57% at depths of 15 cm and 30 cm, respectively. Furthermore, at a horizontal distance of 30 cm, the gravimetric moisture content was detailed at 26.31%, which further declined to 25.38% and 24.64% at the 15 cm and 30 cm depths, respectively. When moving horizontally 30 cm away from the center of the dripper, the gravimetric moisture content was recorded at 25.38% and gradually decreased with depth to 25.27% and 24.96% for depths of 15 cm and 30 cm respectively. It is clear from the above for the moisture distribution coefficients of drip irrigation that the moisture is at its highest in the surface layer below the dripper and

begins to decrease gradually with depth and also horizontally from the center of the dripper for all the previous coefficients. The contour maps reflect a non-linear behavior of water movement within a non-homogeneous porous medium. Therefore, the results showed a transformation of the system from a semi-steady state to a dynamic state dominated by high gradients, which is consistent with Darcy's law and Richards' equation. The pronounced curves in the contour lines also indicate spatial variation in the soil's hydraulic properties, reflecting the effect of its fine texture and heterogeneity on flow paths. These phenomena are likely due to a change in the relationship between moisture content and water conductivity, leading to nonlinear behavior and preferential water transport within the soil. This aligns with the findings of Idam (2001), Al-Saadoun (2006), and Al-Janabi (2012),and Mandal, at al(2025) who observed that moisture content increases at the drip source and decreases with distance from it, whether horizontally or vertically.

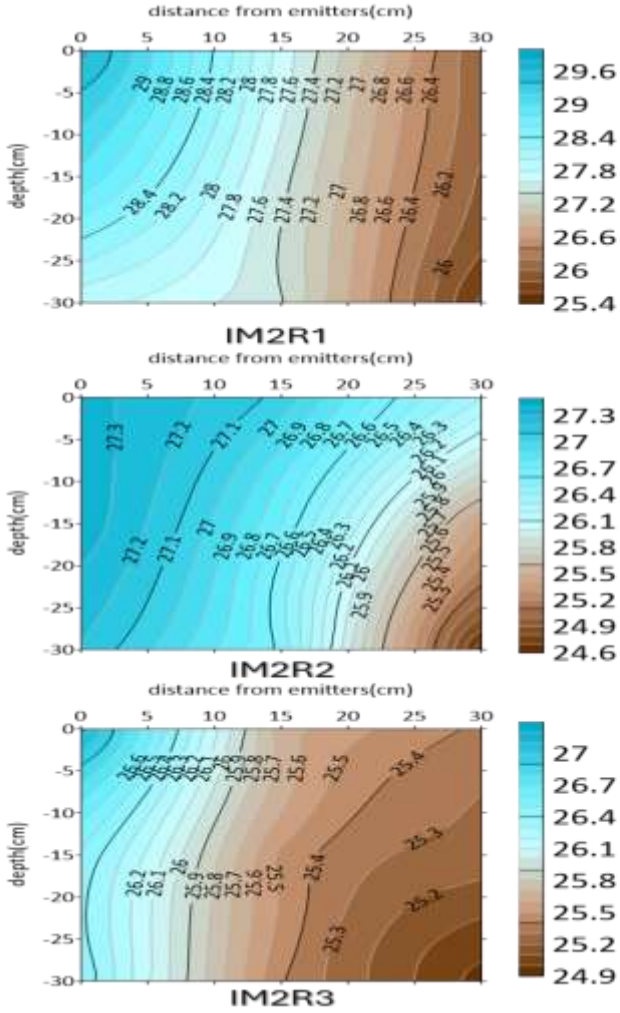

Figure 5. Spatial distribution of soil moisture under smart irrigation management, maintained at 75% of field capacity.

Salinity distribution: dS m⁻¹

The outcomes presented in Figure 6 depict the salinity distribution under the conventional irrigation treatment (CM1) at the 50% irrigation level in the first replicate. The lowest salinity values were documented directly under the center of the dripper, where the electrical conductivity reached 0.88 dS m^{-1} in the surface layer, increasing to 1.38 and 1.41 dS m^{-1} at depths of 15 cm and 30 cm, respectively. At a horizontal distance of 15 cm from the dripper center, salinity values increased to 1.95 dS m^{-1} in the surface layer and to 2.14 and 3.11 dS m^{-1} at depths of 15 cm and 30 cm, respectively. An extra increase in salinity was detected at a horizontal distance of 30 cm from the dripper center, where the electrical conductivity reached 4.38 dS m^{-1} in the surface layer and 4.68 and 4.98 dS m^{-1} at depths of 15 cm and 30 cm, respectively. These outcomes indicate a progressive increase in salinity with increasing horizontal distance from the dripper and, to a lesser extent, with soil depth.

In the second replicate, the lowest salinity level was recorded in the surface layer directly beneath the center of the dripper, where the electrical conductivity reached 0.56 dS m^{-1}, increasing to 1.15 and 1.47 dS m^{-1} at soil depths of 15 cm and 30 cm, respectively. At a horizontal distance of 15 cm from the dripper center, salinity values increased to 2.02 dS m^{-1} in the surface layer and to 2.13 and 2.58 dS m^{-1} at depths of 15 cm and 30 cm, respectively. A further increase was observed at 30 cm from the dripper center, where salinity reached 3.77 dS m^{-1} in the surface layer and 3.34 and 4.92 dS m^{-1} at depths of 15 cm and 30 cm, respectively.

As for the third repeat, the lowest salt concentration in the surface layer below the center of the dripper was ds 0.63, and it was 0.72 and 1.06 dS/m-1 for depths of 15 cm and 30 cm respectively. At a horizontal distance of 15 cm from the center of the dripper, the salinity level reached 1.27 dS m^{-1} in the surface layer, increasing to 2.72 and 2.81 dS m^{-1} at soil depths of 15 cm and 30 cm, respectively. At a further distance of 30 cm from the dripper center, salinity values rose to 2.85 dS m^{-1} in the surface layer and to 3.04 dS m^{-1} at depths of 15 cm and 30 cm, respectively. The convergence of contour lines in the transition zone reflects a salinity front resulting from the interaction of water and salt transport processes. Salts are transported with water through advective flow and also separate due to concentration gradients. Nevertheless, the predominance of water movement toward drier areas promotes salt accumulation in those areas. Accordingly, Figure 6 clearly exhibits an inverse relationship between soil moisture and salinity distribution, where reductions in moisture content are related with increases in salt concentration as a result of transport processes and solute accumulation within the porous soil medium.

The outcomes presented in Figure 7 explain the salinity distribution under the conventional irrigation treatment (CM2) at 75% irrigation level. In the first replicate, the lowest salinity value was documented in the surface layer directly beneath the center of the dripper, where the electrical conductivity reached 1.55 dS m^{-1}, increasing to 2.15 and 2.25 dS m^{-1} at soil depths of 15 cm and 30 cm, respectively. At a horizontal distance of 15 cm from the dripper center, salinity values increased to 2.72 dS m^{-1} in the surface layer and to 2.96 and 3.53 dS m^{-1} at depths of 15 cm and 30 cm, respectively. A further increase was observed at 30 cm from the dripper center, where salinity reached 3.73 dS m^{-1} in the surface layer and 4.53 dS m^{-1} at a depth of 15 cm (and the corresponding deeper layer, respectively).

In the second replicate, the lowest salt concentration in the surface layer below the center of the dripper was 0.87 dS/m-1, and it was 2.04 and 2.2 dS/m-1 for depths of 15 cm and 30 cm respectively. Salinity increased with increasing horizontal distance from the center of the dripper. At 15 cm from the dripper center, salt concentrations were 2.7 dS m^{-1} in the surface layer and 3.41 and 3.42 dS m^{-1} at depths of 15 and 30 cm, respectively. At 30 cm from the dripper center, the corresponding values increased to 3.65, 3.70, and 4.50 dS m^{-1} for the surface, 15 cm, and 30 cm soil depths, respectively.

In the third replicate, the lowest salt concentration in the surface layer below the center of the dripper was 0.55, and it was 0.75 and 1.2 dS/m-1 for depths of 15 cm and 30 cm respectively. Salinity increased with increasing horizontal distance from the dripper center. At 15 cm, salt concentrations were 1.6, 1.9, and 2.2 dS m^{-1} in the surface layer and at depths of 15 and 30 cm, respectively. At 30 cm, the consistent values increased to 3.1, 3.5, and 3.5 dS m^{-1}. Moreover, the contour maps revealed a pronounced spatial gradient in the investigated soil properties, characterized by higher values on the left side (orange) and progressively lower values toward the right side (purple). The close resemblance among the contour patterns refer that these properties were primarily controlled by the movement of water through the soil profile.

When these results are linked with Figure 3, which shows the moisture distribution, it becomes clear that moisture content is the controlling factor in the redistribution of these properties, as the areas with higher moisture content lead to an increase in the solubility of salts and their movement through mass flow and diffusion, which contributes to reducing their concentrations or redistributing them away from those areas. Equally, areas with lower soil moisture were described by reduced leaching efficiency, increased evaporation, and intensified capillary rise of dissolved salts, promoting salt accumulation and elevated salinity levels. The region of contour-line convergence parallels to the wetting front, which marks an abrupt change in soil water potential and delineates the boundary between wetter and drier soil regions. This zone is the most active in terms of water movement. Thus, the shape reflects an integrated system in which the movement of water within the soil controls the spatial distribution of chemical and physical properties, confirming that the moisture gradient is the primary driver of spatial variation, and that the efficiency of irrigation management plays a crucial role in controlling this distribution and limiting salt accumulation.

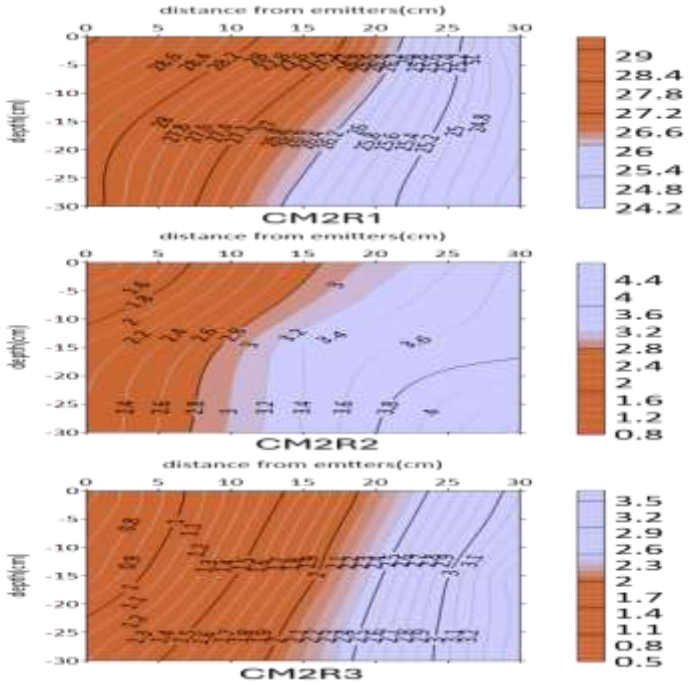

Figure 7. Spatial distribution of soil salinity under the smart irrigation treatment at 75% of field capacity.

The outcomes presented in Figure 8 illustrate the salinity distribution of the smart irrigation (IM1) 50% treatments in the first replicate. The lowest salt concentration in the surface layer below the center of the dripper was 0.93 dS/m-1 and 1.25 dS/m-1 for depths of 15 cm and 30 cm respectively. At a horizontal distance of 15 cm from the the dripper center, the concentration of salinity was 1.27 dS m^{-1} in the surface layer and increased slightly to 1.33 and 1.35 dS m^{-1} at depths of 15 and 30 cm, respectively. At a horizontal distance of 30 cm from the dripper center, the salinity concentration increased markedly to 5.15 dS m^{-1} in the surface layer and to 6.30 and 8.69 dS m^{-1} at depths of 15 and 30 cm, respectively.
For the second replicate, the lowest salinity concentration under the center of the dripper was documented in the surface layer (1.11 dS m^{-1}), while values of 2.16 and 1.23 dS m^{-1} had detected at depths of 15 and 30 cm, respectively. At a horizontal distance of 15 cm from the dripper center, the salinity concentration was 1.39 dS m^{-1} in the surface layer and increased to 2.35 and 2.42 dS m^{-1} at depths of 15 and 30 cm, respectively. At a horizontal distance of 30 cm from the dripper center, the salinity concentration reached 3.23 dS m^{-1} in the surface layer and 3.41 and 3.25 dS m^{-1} at depths of 15 and 30 cm, respectively.
In the third replicate, the lowest salt concentration in the surface layer below the center of the dripper was 0.51 dS/m-1, and it was 1.24 dS/m-1 and 1.3 dS/m-1 for depths of 15 cm and 30 cm respectively. By moving 15 cm horizontally from the center of the dripper, the salt concentration was 1.36 dS/m-1 for the surface layer and 1.53 and 2.52 dS/m-1 for depths of 15 cm and 30 cm. But when moving 30 cm horizontally from the center of the dripper, the salt concentration was 2.74 dS/m-1 for the surface layer and 3.28 and 3.48 dS/m-1 for depths of 15 cm and 30 cm. Figure 8 shows a clear spatial gradient for several soil properties, with relatively low values prevailing on the left side, while values gradually rise towards the right side, with a narrow transitional area where contour lines converge noticeably, indicating a sharp change in values within a short distance. This pattern reveals the impact of a dominant dynamic factor, and when linked to Figure 4, which shows the moisture distribution, it becomes clear that this factor is the water content and the movement of water within the soil. In areas with higher moisture, the movement of water and dissolved ions increases due to mass flow, which leads to the transfer and accumulation of salts and dissolved substances in a certain direction, which explains the high values on the opposite side. Equally, less moist regions experience limited water leaching, with increased evaporation and capillary salt upwelling, resulting in low or slow water potential gradients. The convergence of contour lines in the central region indicates an active wettability region, representing the boundary between the zones of relative saturation and relative dryness. Here, the water potential gradient is high, making this region the most influential in salt redistribution and its associated properties. Therefore, Figure 4 clearly reflects that moisture distribution is the governing factor in shaping this spatial pattern, through its direct influence on dissolution, transport, and concentration processes, which underscores the importance of irrigation management in controlling soil property variation and reducing unwanted salt accumulation.

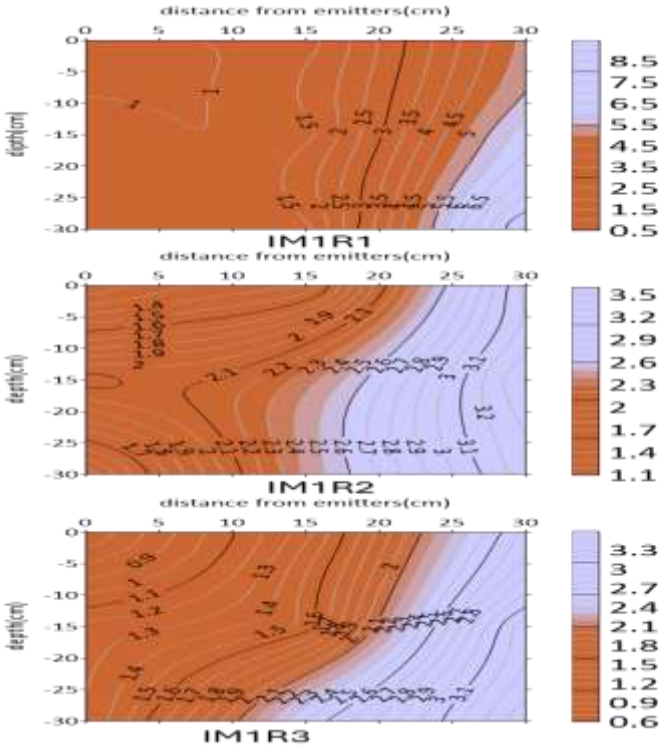

Figure 8. Shows the salinity distribution for smart irrigation treatment at 50% of field capacity.

Figure 9 shows the salt distribution for smart irrigation (IM2) 75% treatments. In the first replicate, the lowest salt concentration in the surface layer below the center of the dripper was 0.81 dS/m-1, and it was 1.6 and 1.8 dS/m-1 for depths of 15 cm and 30 cm respectively. For a distance of 15 cm horizontally from the dripper center, the salinity concentration was 1.9 dS/m-1 at the surface and 1.9 and 2.2 dS/m-1 for 15 cm and 30 cm depth respectively. For a distance of 30 cm horizontally from the dripper center, the salinity concentration was 3.2 dS/m-1 at the surface and 3.4 and 3.6 dS/m-1 for 15 cm and 30 cm depth respectively.

For the second replicate, the minimum salt concentration at the surface layer at 15 cm and 30 cm from the center of the dripper was 1.12 dS/m-1, while that at depths of 15 cm and 30 cm was 1.31 and 2.09 dS/m-1, respectively. For the distance of 15 cm from the center of the dripper horizontally, the salt concentration was 3 dS/m-1 at the surface layer and 3.24 and 3.69 dS/m-1 at depths of 15 cm and 30 cm, respectively. For the distance of 30 cm from the center of the dripper horizontally, the salt concentration was 3.92 dS/m-1 at the surface layer and 4.11 and 4.68 dS/m-1 at depths of 15 cm and 30 cm, respectively.

On the third replicate, the lowest concentration of salt in the surface layer under the dripper center was 0.95 dS/m-1, whereas in the soil layer at 15 cm and 30 cm depths, the salt concentration was 1.06 and 1.2 dS/m-1. On horizontally moving 15 cm away from the dripper center, the salt concentration in the surface layer was 1.25 dS/m-1, whereas the salt concentration was 1.25 and 1.31 dS/m-1 in the soil layer at 15 cm and 30 cm depths. On horizontally moving 30 cm away from the dripper center, the salt concentration in the surface layer was 2.82 dS/m-1, whereas in the soil layer at 15 cm and 30 cm depths, the salt concentration was 2.95 and 3.25 dS/m-1. Figure 9 shows a clear spatial gradient for several soil properties, with relatively low values prevailing on the left side (orange), while they gradually increase towards the right side (purple), with a narrow transitional area emerging where the contour lines converge noticeably, indicating a sharp change in values within a limited distance. This pattern reflects the dominance of a major physical factor, which is the movement of water within the soil. Once this figure is associated with Figure 5 of moisture distribution, it is evident that the amount of water is the key determinant in determining this gradient, whereby places with high humidity result in the facilitation of mass flow of water and dissolved ions, which in turn results in the transport of salts and dissolved substances to certain locations, causing the increased concentration on the right-hand side. In contrast, for areas with low moisture content, the effects are poor water leaching and high evaporation and capillary rise, which leads to relatively low values or slow changes in those values. Additionally, the convergence of the contour lines in the central area shows the active wetting front, which is marked by high water potential gradient and high water and ion transport rates. Therefore, the figure reflects a dynamic system in which the properties of moisture distribution (Figure 5) control the direction of dissolution, transport and concentration processes, confirming that irrigation management and water distribution efficiency play a crucial role in controlling the spatial variability of soil properties and limiting salt accumulation.

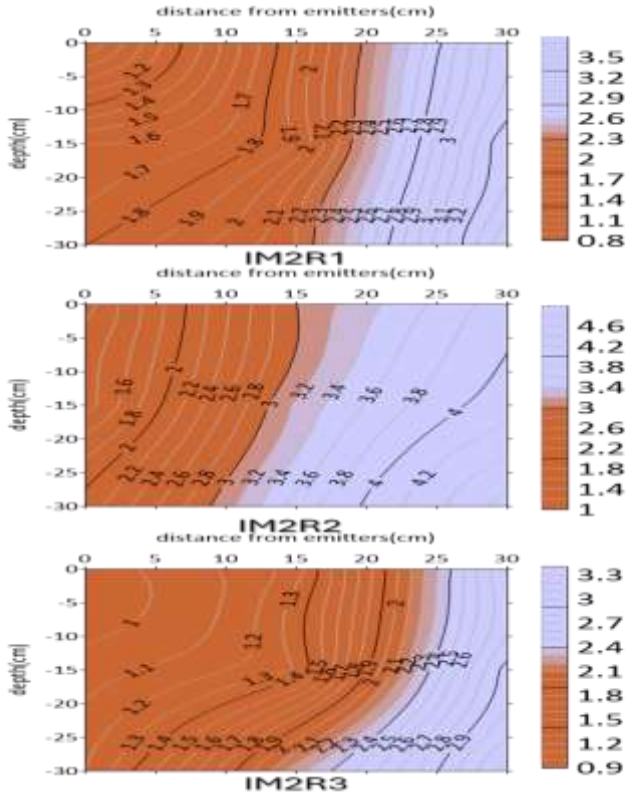

Figure 9. Shows the salinity distribution for smart irrigation treatment at 75% of field capacity.

Conclusion

The moisture distribution results demonstrated that the highest moisture contents were concentrated directly beneath the emitter and gradually decreased with increasing horizontal and vertical distances from the water application source. This finding confirms that water movement within the soil profile was governed by gradients in water potential and the hydraulic properties of the soil, with horizontal variations in moisture being more pronounced than vertical variations. The contour maps of moisture distribution revealed that the smart irrigation system achieved a more uniform distribution of soil moisture compared with the conventional irrigation system. This improvement was attributed to the use of soil moisture sensors and real-time water application management, which reduced the occurrence of excessively dry or saturated zones within the root zone. The results also indicated a clear inverse relationship between soil moisture content and salt distribution. Salt concentrations increased in areas with lower moisture content due to reduced leaching efficiency and the enhanced effects of evaporation and capillary rise, whereas salt concentrations decreased in regions characterized by higher levels of wetting.

References

1- Al-Janabi, Muhammad Ali Aboud Faris. 2012. The Effect of Drip Irrigation and Organic Fertilization on the Growth and Yield of Potatoes (Solanum tuberosum L.). PhD Dissertation. College of Agriculture. University of Baghdad.

2- Al-Saadoun, Jamal Nasser Abdulrahman. 2006. The effect of some drip irrigation parameters on water and salt distribution in clayey alluvial soils and on okra crop production. PhD dissertation. College of Agriculture. University of Baghdad.

3- Aydam, Jawad Kadhim. 2001. The effect of the shape and lateral slope of the ridge on the pattern and distribution of salts in soils under different irrigation methods. PhD dissertation. College of Agriculture. University of Baghdad.

4- Faleh, S. T., Abood, M. A., and Fahmi, A. H. 2023. The Role of Biochar and Perlite in Improving some Physical Properties of Clay Loam and Sandy Loam Soil. In IOP Conference Series: Earth and Environmental Science (Vol. 1259, No. 1, p. 012020). IOP Publishing.

5- Gaitan, N. C., Batinas, B. I., Ursu, C., and Crainiciuc, F. N. 2025. Integrating Artificial Intelligence into an Automated Irrigation System. Sensors, 25(4), 1199.

6- Ghazi, N. M., Tahir, H. T., Othman, S. S., Hawar, D. A., Abdulkadir, M. A., and Korkmaz, C. 2025. Smart irrigation systems: A comprehensive review of IoT, AI, and sustainable agriculture technologies.

7- Jones, H. G. 2004. Irrigation scheduling: advantages and pitfalls of plant-based methods. Journal of experimental botany, 55(407), 2427-2436.

8- Ma, S., Tong, L., Kang, S., Wang, S., Wu, X., Cheng, X., and Li, Q. 2022. Optimal coupling combinations between dripper discharge and irrigation interval of maize for seed production under plastic film-mulched drip irrigation in an arid region. Irrigation Science, 40(2), 177-189.

9- Mandal, D., Khosla, R., Longchamps, L., and Joshi, D. 2025. Soil moisture sensor location-allocation using spatial association of surface moisture data. Smart Agricultural Technology, 11, 100929.
10- Montzka, C., Brocca, L., Chen, H., Das, N. N., Dasgupta, A., Rahmati, M., and Jagdhuber, T. 2026. AI in soil moisture remote sensing. International Journal of Applied Earth Observation and Geoinformation, 146, 105011.
11- Nurmalitasari, N., Nurchim, N., and Lestari, R. D. 2025. Artificial Intelligence-Driven Solar Smart Irrigation for Sustainable Agriculture: Trends, Challenges, and SDG Implications–A Systematic Review. Smart Agricultural Technology, 101665.
12- Richards, L. A. (Ed.). 1954. Diagnosis and improvement of saline and alkali soils (No. 60). US Government Printing Office.
13- Salam, Osama. 2023. Artificial Intelligence in Addressing Water and Climate Issues. Arab Republic of Egypt. Erteqa for International Publishing and Distribution.
14- Sharma, A., Jain, A., Gupta, P., and Chowdary, V. 2020. Machine learning applications for precision agriculture: A comprehensive review. IEEe Access, 9, 4843-4873.
15- Zhang, H., Zhao, J., Hong, M., and Ma, L. 2025. Optimization of deficit irrigation system for drip-irrigated corn in northern Xinjiang using dynamic reconstruction and dual physics-informed neural networks to drive AquaCrop. Frontiers in Plant Science, 16, 1678277.
16- Zhang, W., Xiong, Y., Li, Y., Qiu, Y., and Huang, G. 2022. Effects of organic amendment incorporation on maize (Zea mays L.) growth, yield and water-fertilizer productivity under arid conditions. Agricultural Water Management, 269, 107663.